Dually Charged MOF-based Thin-film Nanocomposite Nanofiltration Membrane for Enhanced Removal of Charged Pharmaceutically Active Compounds

Ruobin Dai,[†] Xueye Wang,[†] Chuyang Y. Tang,[‡] and Zhiwei Wang[*,†]

[†] State Key Laboratory of Pollution Control and Resource Reuse, Shanghai Institute of Pollution Control and Ecological Security, School of Environmental Science and Engineering, Tongji University, Shanghai 200092, China

[‡] Department of Civil Engineering, the University of Hong Kong, Pokfulam Road, Hong Kong S.A.R., China

[*] To whom all correspondence should be addressed.

Tel.: +86-21-65975669, Fax: +86-21-65980400, E-mail address: zwwang@tongji.edu.cn

Revised manuscript submitted to *ES&T* (Clean version)

ABSTRACT

Removal of pharmaceutically active compounds (PhACs) is of great importance in wastewater reclamation due to their potent negative impact on human health. Typical polyamide nanofiltration (NF) membranes are negatively charged, which compromises their rejection rate of positively charged PhACs. Herein, we propose to rationally design a novel thin-film nanocomposite (TFN) NF membrane featuring dually charged metal organic framework (MOF) to effectively remove both positively and negatively charged PhACs. Ethylenediamine (ED) was grafted to the coordinately unsaturated metal sites inside the MIL-101(Cr). The resulting ED-MIL-101(Cr) contained both amine groups inside its channels to provide strong positive charge and negatively charged carboxyl groups at its surface. This dually charged nature of the MOF nanoparticles enabled the ED-MIL-101(Cr)-containing TFN membrane to achieve high rejection rates (mostly >90%) for both positively (terbutaline, atenolol, fluoxetine) and negatively charged PhACs (ketoprofen, diclofenac, bezafibrate). At the same time, the ED-MIL-101(Cr) TFN membrane had greatly improved water permeance (140% over the control membrane with MOF loading). Calculations based on density functional theory further confirmed the large energy barrier for the migration of both negatively and positively charged PhACs across the nanochannels of ED-MIL-101(Cr). This study highlights a promising potential of dually charged MOF-TFN membranes for efficient removal of trace organic contaminants in wastewater reclamation.

34 **TOC Art**

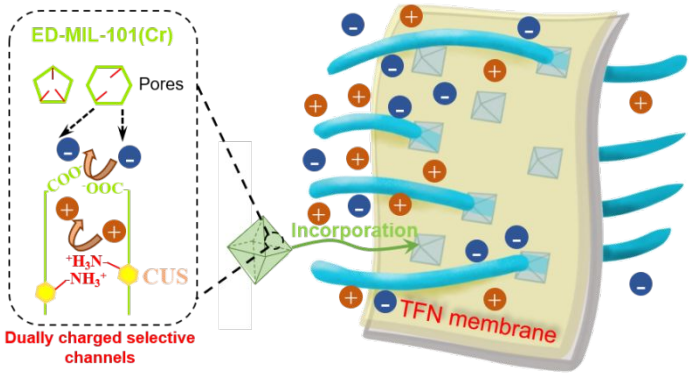

35

36

INTRODUCTION

Wastewater reclamation, as an effective route of sustainable water resource management, is of great importance for addressing the increasing crisis of water scarcity.[1–5] Pharmaceutically active compounds (PhACs) are extensively used in daily life and their presence in secondary-treated wastewater or natural water systems is inevitable, resulting from inefficiency of current wastewater treatment processes.[6,7] Although PhACs are generally present at trace concentrations of ng - μg L^{-1}, they can cause potent adverse effects such as reproductive and neural toxicological effects or carcinogenicity on humans and other organisms through drinking water and food chains.[7,8] Therefore, removal of PhACs is of great significance prior to water reuse.[5,9,10]

Nanofiltration (NF) is an attractive membrane separation process for wastewater reclamation,[11,12] which has the potential for the removal of PhACs.[13–15] The rejection of charged PhACs by NF is mainly based on size (steric) exclusion and electrostatic interactions.[16,17] Typical thin-film composite (TFC) polyamide (PA) NF membranes have relatively high rejection rate of negatively charged PhACs ($PhACs^-$) but compromised rejection of positively charged PhACs ($PhACs^+$) at neutral pH,[16–18] ascribing to negatively charged carboxyl groups in their PA active layer. Reducing the pore size of a NF membrane can effectively enhance its rejection of $PhACs^+$,[16,19] yet at the cost of sacrificing the membrane water permeance and increasing the operating pressure. Other alternatives, such as tuning the surface charge of the membrane by grafting positively charged functional groups, can increase rejection of $PhACs^+$ but compromise the rejection of $PhACs^-$.[20] Introducing zwitterions onto the surface of membrane may facilitate rejection of both $PhACs^-$ and $PhACs^+$ but often results in a significant

decrease of water permeance.[21] Therefore, developing more versatile strategies that increase the membrane rejection of both PhACs$^+$ and PhACs$^-$ without losing water permeance are of great fundamental and practical significance.

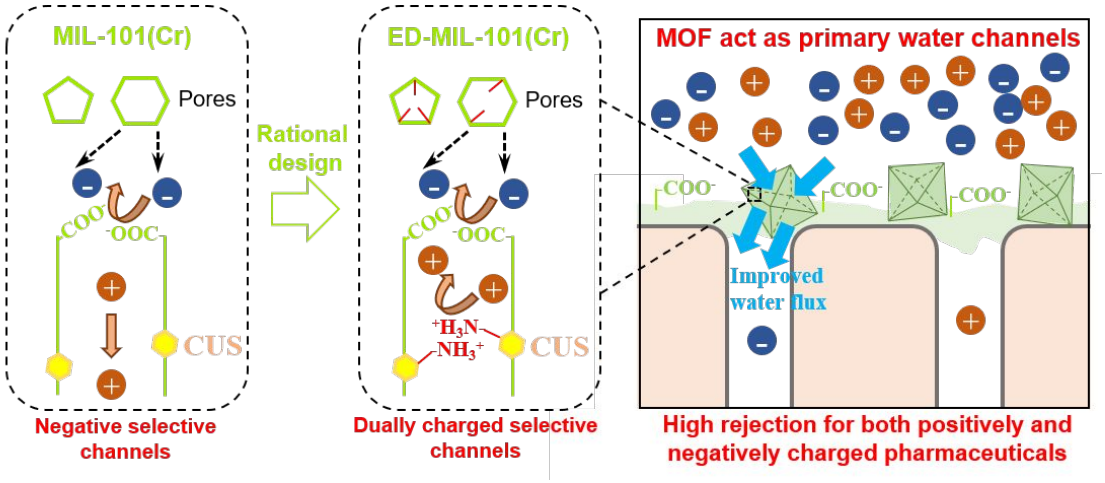

Figure 1. Schematic of a dually charged MOF thin-film nanocomposite nanofiltration membrane for charged PhACs removal by rational design of MOF nanofiller. MIL-101(Cr) has negatively charged -COO^- groups on its surface that repel negatively charged PhACs$^-$. By grafting ethylenediamine (ED) onto the Cr coordinately unsaturated metal-sites (CUS) of MIL-101(Cr) (Supporting information S1), the resulting ED-MIL-101(Cr) attains a dual charge property. The dually charged MOF TFN membrane has high rejection against both positively and negatively charged PhACs, with PhACs$^+$ rejected by the positively charged -NH_3^+ groups in the internal water channels of ED-MIL-101(Cr) and PhACs$^-$ rejected by its negatively charged -COO^- groups at its surface.

Incorporating nanoparticles (NPs) into the PA active layer (a typical route of interface engineering[22]), *i.e.*, forming a thin-film nanocomposite (TFN) membrane,[23] to provide additional nanochannels is a promising way to tune the membrane selectivity without compromising its water permeance.[24,25] Interestingly, MIL-101(Cr), a kind of metal organic

frameworks (MOFs),[26] can dominate the separation properties of the MOF-incorporated TFN membrane by routing water passage through the abundant water channels of MIL-101(Cr)[24]. This observation prompts us to further investigate the feasibility of enhancing the removal of PhACs by rationally designing the nanochannels of MOFs. Presumably, the negatively charged carboxyl groups at the surface of MIL-101(Cr) enable high rejection of $PhACs^-$. Furthermore, inspired by the concept of Janus membranes[27,28], we hypothesize that MOFs with a dual charge property (*e.g.*, with negative surface charges and positive internal charges) can enhance the rejection against both positively and negatively charged PhACs. In this novel strategy (Figure 1), in addition to the rejection of $PhACs^-$ by the surface carboxyl groups, the positive charged internal water channels provide a strong barrier to $PhACs^+$.

In this study, we report a novel dually charged MOF-TFN membrane for enhanced removal of PhACs. MOF NPs of ED-MIL-101(Cr) with dual charge property, prepared by grafting ethylenediamine (ED) onto the Cr coordinately unsaturated metal-sites (CUS) of MIL-101(Cr), were used for the preparation of the MOF-TFN membrane. Its rejection of both negatively and positively charged PhACs was systematically studied. The pristine and sulfonic acid groups grafted MIL-101(Cr) were used as control to resolve the critical role of the grafted ED groups. Calculation based on the density functional theory provides additional insights into the interaction between charged PhACs and the dually charged MOF ED-MIL-101(Cr). The results present a promising MOF-TFN membrane for efficient rejection of PhACs in wastewater reclamation.

MATERIALS AND METHODS

Materials and Chemicals. The substrate for forming PA selective layer was a commercially available polyethersulfone (PES) ultrafiltration membrane (LX-300K, Synder Filtration, MWCO = 300 kDa), which was treated with 20% isopropanol for 30 min before further use. Mesoporous Cr-BDC MOF MIL-101(Cr) nanoparticles with 1.2 nm pentagonal/1.6 nm hexagonal openings were synthesized according to Wang et al[29]. Ethylenediamine (ED, ≥99%) and aminomethanesulfonic acid (AMSA, 98%) used for the grafting were provided by Sinopharm Chemical Reagent Co., Ltd. Toluene (anhydrous) and ethanol (absolute) were purchased from Macklin. Piperazine (PIP, 99%), trimesoyl chloride (TMC, 98%), and *n*-hexane (≥98%) from Aladdin were used for interfacial polymerization (IP) to form the PA layer. Sodium chloride, calcium chloride, and sodium sulfate used for salt rejection evaluation were obtained from Macklin. Six PhACs were used in this study, including three negatively charged compounds (ketoprofen, diclofenac and bezafibrate) and three positively charged ones (terbutaline, atenolol and fluoxetine). Terbutaline (98%) and ketoprofen (≥98%) were purchased from Aladdin, and atenolol (≥98%), fluoxetine (98%), diclofenac (98%), and bezafibrate (99%) were obtained from Macklin. The physicochemical properties of the PhACs are summarized in Table S1. Dextrose (180 Da) from Macklin was used as surrogate for determining the effect of size exclusion of the NF membranes. Citrate-stabilized 5 nm gold nanoparticle (GNP) solution was provided by BBI Solutions (UK). All chemicals were used as received.

MOF Grafting and Characterization. MIL-101(Cr) MOFs were used for selectively filtrating PhACs/water mixture due to their suitable pore size (Supporting Information, Section S1). Grafting of functional groups onto Cr CUSs of MIL-101(Cr) was conducted according to

literature.[30–32] ED and AMSA were used as sources of -NH_2 and -SO_3H functional groups, respectively. Before functionalization, the as-synthesized MIL-101(Cr) was vacuum-treated at 150 °C for 12 h to generate CUSs by removing the bonded water molecules. Dehydrated MIL-101(Cr) (0.3 g) was suspended in 30 mL anhydrous toluene with addition of 0.75 mmol ED or AMSA. The mixture was refluxed for 12 h with a continuous stirring. The product was filtered, purified by ethanol/water and dried at 40 °C vacuum oven. The ED and AMSA grafted products were denoted as ED-MIL-101(Cr) and AMSA-MIL-101(Cr), respectively (Supporting Information, Section S1).

The morphology of the pristine and grafted MIL-101(Cr) was observed by field emission scanning electron microscopy (FESEM, Hitachi S-4800), and the size of MOFs in SEM images was determined by software Nano Measurer 1.2 (developed by Jie Xu, Fudan University). The crystalline structure of MOFs was confirmed by X-ray powder diffraction pattern (XRD, Bruker D8 ADVANCE diffractometer) with Cu Kα radiation (λ=1.54056 Å). Fourier transform infrared spectroscopy (FTIR) was used to investigate the molecular structure of MOFs using KBr pellets. BET surface area of the MOFs was determined via a micromeritics surface area and porosity analyzer (ASAP 2460).

Membrane Fabrication and Characterization. The PES substrate (10 cm × 15 cm) was firstly fixed between two identical custom-designed stainless-steel frames. An aqueous solution of 1.0 wt% PIP was poured onto the surface of the substrate for 2 min contact. After removal of excess PIP solution using filter papers, the upper surface of the substrate was further exposed to a 0.15 wt% TMC/*n*-hexane solution for 30 s reaction to form thin-film composite (TFC) PA active layer. The membrane was drained for 2 min after pouring off the TMC/*n*-hexane solution.

The TFC membrane was then rinsed with *n*-hexane and DI water, followed by 10 min thermal treatment in 50°C hot water. After these post-treatment process, the membrane was stored in DI water at 4°C for further characterization or use. The TFC membrane fabricated herein was denoted as NFcontrol.

For MOF-TFN membrane fabrication, 0.08 wt/v % MOF (MIL-101(Cr), ED-MIL-101(Cr), or AMSA-MIL-101(Cr)) was dispersed in the TMC/*n*-hexane solution via 30 min ultrasonication at room temperature prior to IP. The other reaction and post-treatment procedures were similar to those for fabricating TFC membranes. The resulting TFN membranes were denoted as MIL-TFN, ED-TFN, and AMSA-TFN membranes, respectively, in accordance to the type of MOF nanoparticles used.

An FESEM (Hitachi S-4800) was used to observe the surface and cross-sectional morphologies of membranes. X-ray photoelectron spectroscopy (XPS), zeta potential, and GNP-transmission electronic microscope (TEM) characterizations of the membranes were documented in our previous work.[24,33]

Filtration Experiments. The performance of TFC and MOF-TFN NF membranes were evaluated in a laboratory-scale cross-flow filtration system, as detailed previously.[24] A 5 L feed solution of DI water was recirculated for 4 h for membrane precompaction at 11 bar at a cross-flow velocity of 20.0 cm/s. The pure water flux was then measured at 8 bar. To test the rejection of a single salt (NaCl, $CaCl_2$, or Na_2SO_4), the corresponding salt with concentration of 10 mM was added, followed by stabilization for 2 h and testing at 8 bar. After these measurements, the feed solution was replaced with DI water and stock solution of six PhACs was spiked into the feed tank to form a concentration of 200 μg/L for each compound, while the pH of the feed tank

was adjusted to 7. As the concentration of hundreds μg/L has been widely used in the research related to micropollutant removal by advanced membranes[12,34,35], and in fact concentration of some micropollutants can reach levels of μg/L in real effluents[36,37], we therefore selected 200 μg/L concentration for evaluating the performance of MOF-TFN membranes. In order to exclude the effect of background adsorption on the rejection profile, the experiments were then continued for an additional 12 h, which is longer than the adsorption saturation time of several hours reported in literature[24,34,38]. Then the samples of PhACs were collected from the feed and permeate. The protocol for the rejection of dextrose was the same as the above procedures, except that the feed concentration was 40 mg/L (TOC). All the filtration tests were repeated for at least three times.

Instrumental Analysis for PhACs. The concentrations of PhACs were determined using high-performance liquid chromatography tandem quadruple mass spectrometry (LC-MS/MS, Thermo TSQ Quantum) equipped with a C18 column (Agilent, 5 μm, 150 × 4.6 mm). The MS/MS scan was performed in multiple reaction monitoring mode. The detailed information is given in Supporting Information, Section S2.

Density Functional Theory Calculations. The interaction between ED-MIL-101(Cr) and two model PhACs (atenolol (+) and ketoprofen (-), Figure S2) was investigated using first-principles with the projected-augmented-wave (PAW) method and the GGA-PBE functional based on density functional theory (DFT). Spin-polarized calculations were employed with the double numerical polarization basis set. DFT semi-core pseudopotential was applied for the core-electron treatment. Brillouin zone was sampled by Monkhorst-Pack grid as Γ-point for all systems. The SCF convergence for each electronic energy was set as 1.0×10^{-5} Ha, and the

geometry optimization convergence criteria were set up as follows: 1.0×10^{-5} Ha for energy, 0.004 Ha $Å^{-1}$for force, and 0.01 Å for displacement, respectively. A representative unit of ED-MIL-101(Cr) was chosen for calculation due to a high degree of symmetry in ED-MIL-101(Cr) structure, as shown in Figure S3. In our calculation, the repulsion energy was calculated by the equation: $E_r=E_{total}- E_{Vtotal}-E_1$, where the E_{total} is the total energy of ED-MIL-101(Cr) structure adsorbed with PhACs, E_{Vtotal} is the energy of the ED-MIL-101(Cr) structure and E_1 is the energy of molecule. The migration energy barriers of two PhACs across ED-MIL-101(Cr) structure were calculated using the linear and quadratic synchronous transit (LST/QST) methods in combination with the conjugated gradient (CG) refinement. For all DFT calculations, the solvation effect (H_2O) with solvation model has been employed, considering the presence of water molecules in the systems.

RESULTS AND DISCUSSION

Characterizations of As-Prepared MOFs. Three MOFs including MIL-101(Cr), ED-MIL-101(Cr), and AMSA-MIL-101(Cr) were synthesized, in which both MIL-101(Cr) and AMSA-MIL-101(Cr) were used as control to determine the function of the grafted ED groups. The SEM images (Figure 2a) of the synthesized pristine and grafted MIL-101(Cr) show a nearly identical nanometric crystal size around 160 nm. The crystalline structure of MIL-101(Cr) was confirmed by powder XRD (Figure 2b), with characteristic diffraction peaks at 9.0° and 16.5°.[29] The XRD patterns of ED-MIL-101(Cr) and AMSA-MIL-101(Cr) were nearly identical to that of MIL-101(Cr), suggesting that their crystalline structure were unaffected by grafting process. To evaluate the impact of grafted functional groups on the porous nature of MOFs, the N_2

adsorption-desorption measurement was performed (Figure S4). The BET surface area of MIL-101(Cr), ED-MIL-101(Cr), and AMSA-MIL-101(Cr) was determined to be 2421, 2095 and 2112 m^2/g, respectively, indicating that the porous properties were maintained after grafting (see pore size distribution profiles in Figure S5). The decrease in BET surface area was typically observed after grafting of functional groups for MOFs[30]. The slight decrease in BET surface area might be attributed to the grafted groups ($-NH_2$ or $-SO_3H$), which replaced terminal water molecules onto CUSs[30]. Note that the decrease in BET surface area of MIL-101(Cr) was dependent on the time for amine grafting. If the amine grafting time were prolonged, the decrease in BET surface area of MOF would be more apparent. However, as the ED-MIL-101(Cr) was used as a material for filtration in our study, the BET surface area of ED-MIL-101(Cr) should not be too small to allow water to pass through.

The bands of FTIR (Figure 2c) between 1800-1300 cm^{-1} corresponded to vibrations of C-C and -COO, implying the presence of dicarboxylate linker in MIL-101(Cr). The observed aliphatic C-H stretching vibrations (2800-3000 cm^{-1}) and N-H stretching vibrations (3100-3400 cm^{-1}) were shifted to larger values, indicative of the molecule coordinated to a Lewis acid center[39,40], consistent with the selective ED grafting onto chromium(III) CUSs. For the AMSA-grafted one, it showed signals of sulfonic acid groups at 1207 cm^{-1} and 641 cm^{-1}, corresponding to the symmetric stretching vibrations of S=O and S-O, respectively[31]. Zeta potential measurement (Figure 2d) showed that the MIL-101(Cr) was positively charged at neutral pH even though its surface carboxylic groups are negatively charged. Our result is consistent with earlier studies[24,41], noting that zeta potential measurement can be affected by both the surface and bulk properties for porous materials. After ED grafting, the charge of MOF became more

positive (increase from 7.4 mV to 18.7 mV at pH = ~7), while the MOF after AMSA grafting showed a negative trend. This could result from grafted groups present at the center of mesopore cages according to Hwang *et al.* [30], leading to the location of grafted ED functional groups in the middle of nanochannels of the ED-MIL-101(Cr), with both ends of the nanochannels negatively charged. The dually charged property of ED-MIL-101(Cr) is further analyzed in Section ***Interaction between PhACs and MOFs.***

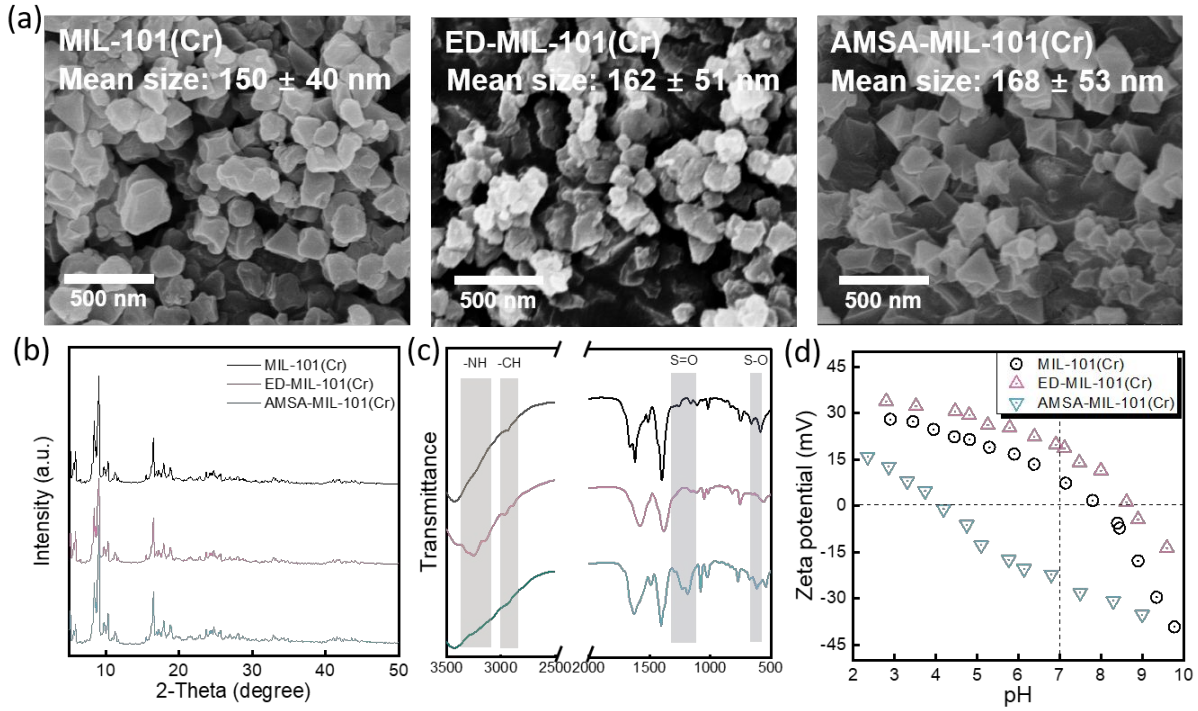

Figure 2. Characterizations of pristine and grafted MIL-101(Cr): (a) SEM; (b) XRD, (c) FTIR and (d) zeta potential. Note that the scale bar of the left side of FTIR images was enlarged three times compared to that of the right side.

MOF-TFN Membrane Characterization. The as-synthesized MOFs were directly incorporated into PA layer during interfacial polymerization to generate MIL-TFN, ED-TFN, and AMSA-TFN NF membranes. Compared to the NFcontrol without embedment of

nanoparticles, the MOF-loaded TFN membranes contained nanoparticles with similar shape and particle size as pristine MOFs or grafted MOF crystals (Figure 3a, SEM). The amounts of the nanoparticles present on membrane surface were comparable among the various MOF-TFN membranes. The cross-sectional SEM images (Figure 3b) clearly show the formation of active layers incorporated by MOFs. Surface roughness of membranes looks different on SEM images. In the existing literature, roughness of polyamide layers has often been correlated to membrane performance[42,43]. Nevertheless, a roughness characterization on TFN membrane is incapable of revealing whether the change in surface roughness is ascribed to the shape of crystalline MOF or the change in polyamide layer in the current study. Moreover, due to the significant difference in water transport characteristics between MOF and polyamide, it is not possible to correlate the change in roughness after MOF incorporation with the transport property of membranes.

The results of XPS survey revealed the presence of chromium on MOF-TFN membranes (Figure 4c), and the amounts of MOFs on the membrane surface were similar (Table S2). The O 1s peak from XPS spectra was further deconvoluted and an additional peak at 530.1 eV associated with chromium species containing coordination bond (C-O*-Cr) provided further evidence of the presence of MOFs in the PA layer for MIL-, ED-, and AMSA-TFN membranes (Figure 4d, Figure S6).

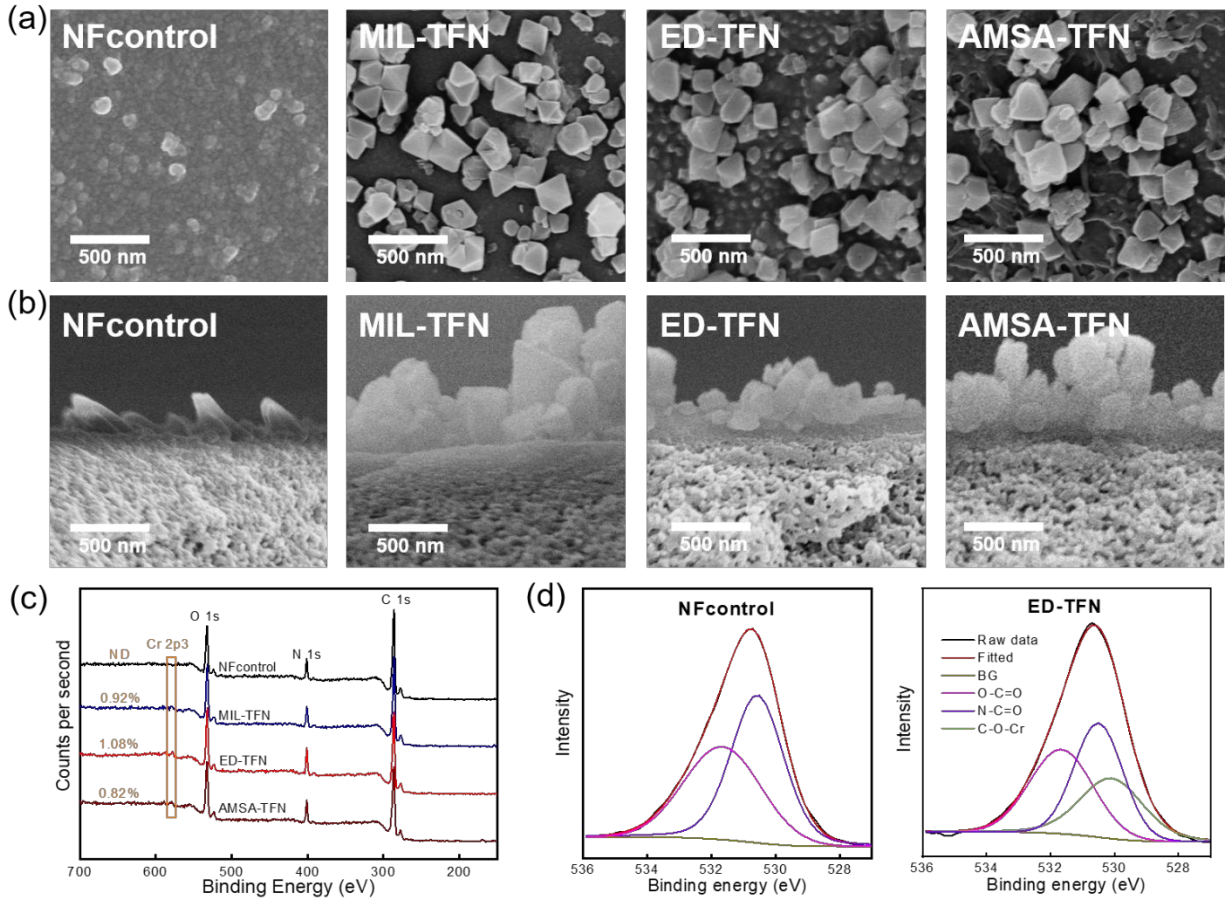

Figure 3. (a) Projected and (b) cross-sectional SEM characterizations of NFcontrol and TFN membranes loaded with different MOFs; (c) XPS spectra and (d) analysis of oxygen 1s in a high-resolution for various membranes.

The incorporation of MOFs into polyamide layer of the membrane significantly increased membrane water permeance from A = 17.3 L m^{-2} h^{-1} bar^{-1} for NFcontrol to A = 22.4-24.6 L m^{-2} h^{-1} bar^{-1} for the MOF-TFN membranes (Figure 4a, Table S3). This significant enhancement was attributed to the nanochannels of the embedded MOFs as the shortcuts for water transport[24]. The MOF-TFN membranes exhibited nanofiltration-like properties[44] with NaCl rejections around 35-37% and A/B_{NaCl} around 0.08 bar^{-1}. These rejection properties are comparable with the NFcontrol membrane (Table S3). Furthermore, compared with membranes recently

developed in literature in terms of water permeance and solute rejection, the performance of MOF-TFN membranes in this study is favorable (Figure S7).

Charge of MOFs Controls Rejection of Charged Solutes by TFN Membranes. We used two additional salts ($CaCl_2$ and Na_2SO_4) to probe the effect of charge properties of MOFs on the membrane separation properties. Rejection of asymmetrically charged salts is governed by the ions with higher valency (*i.e.*, Ca^{2+} for $CaCl_2$ and SO_4^{2-} for Na_2SO_4), because the rate of salt transport is controlled by the electrostatic repulsive or attractive interactions between the high valence ions and the membrane[45,46]. All the membranes achieved a relatively high Na_2SO_4 rejection of approximately 90% (Figure 4b), which can be ascribed to the negative surface charge of these membranes at the test pH (Figure S8). In contrast, the MOF incorporated membranes MIL-TFN, ED-TFN and AMSA-TFN had significantly increased $CaCl_2$ rejection (75.0%, 90.7%, and 66.4%, respectively) compared to that of NFcontrol (48.2%). This enhancement can be partially explained by the dilution effect due to the greater water permeance of the MOF-TFNs. According to the literature[44], increase of water permeation through a membrane tends to dilute the solute concentration in the permeate and thus enhances membrane rejection. Figure 4b also highlights the critical role of electrostatic interactions between the MOFs in the TFN membranes and charged solutes, with the dually charged MOF-TFN membrane ED-TFN showing the highest $CaCl_2$ rejection among all the membranes. In contrast to the AMSA-TFN membrane that partially screens positive charge of CUSs by $-SO_3H$ substitution, the high rejection of ED-TFN to both $CaCl_2$ and Na_2SO_4 implies the crucial effect of dually charged ED-MIL-101(Cr) on the separation performance of the whole membrane, *i.e.*, the dually charged nanochannels of ED-MIL-101(Cr) may act as the primary water transport

296 channel of the ED-TFN membrane.

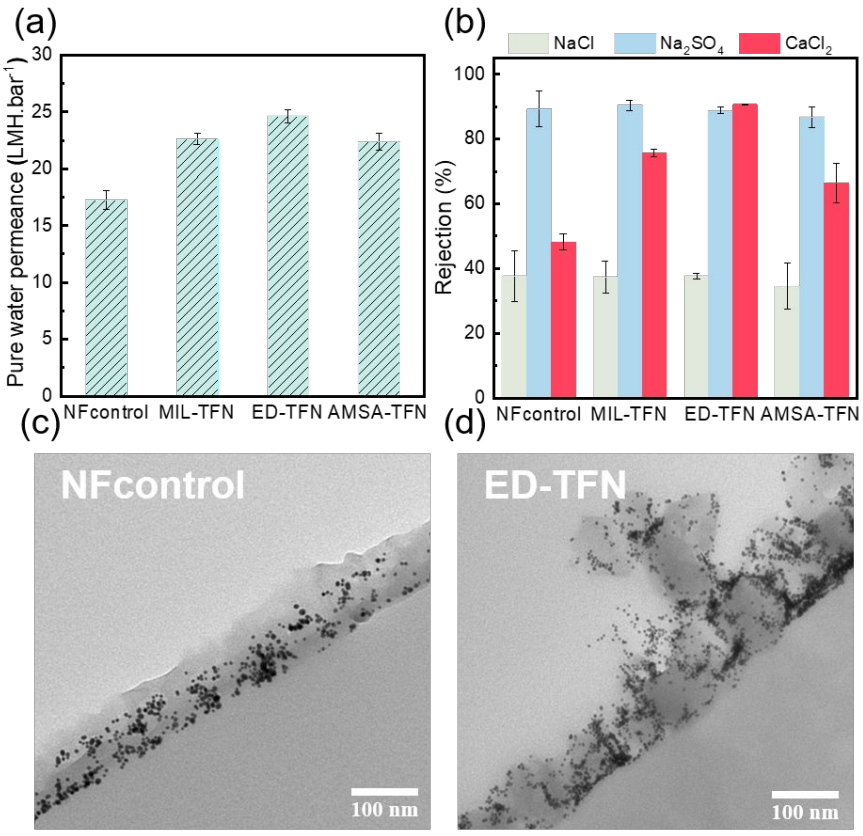

297

298 **Figure 4.** Evidence for critical roles of charge of MOFs in membrane separation properties: (a) Water
299 permeance; (b) Salt rejections, (c-d) Cross-section TEM images of gold nanoparticle deposition on the
300 surfaces of NFcontrol and ED-TFN membranes after 10-min filtration tests (1.0×10^{12} particles/mL, 25°C,
301 5 bar).

302

303 To further identify the primary water transport channels of MOF-TFN membranes, we used
304 GNPs filtration followed by TEM characterization to visualize the spatial distribution of sites
305 for water permeation in the MOF-TFN membranes. Note that a static GNP deposition test in
306 our previous study[24] has eliminate the possibility that local concentrated GNPs around MOFs
307 is induced by difference in affinity between polyamide and MIL-101(Cr). A clear tendency for

GNPs to cluster around the MOF particles was observed (Figure 4d, Figure S10). The size of GNPs used is about 5 nm, which is significantly larger than the pores of MIL-101(Cr) (1.2/1.6 nm). Hence, the GNPs tend to cluster around the MOFs rather than enter into the MOFs, though the water may preferentially pass through the pores of MOFs. Moreover, the MOF-TFN membranes showed an increased rejection of $CaCl_2$ compared to that of NFcontrol membrane (Figure 4b) while the rejection of dextrose kept nearly the same (Figure S9), which demonstrated that the water flux across the TFN membrane mainly passes through the pores of MOFs. These results support our hypothesis that the pores of MOFs served as primary nanochannels in the filtration of the MOF-TFN membrane since GNPs are expected to closely follow the streamlines and are useful markers for identifying water transport pathways[45,46]. Combined with the results of high $CaCl_2$ and Na_2SO_4 rejections (both nearly 90%) by the ED-TFN membrane, the importance of nanochannels in ED-MIL-101(Cr) with dually charged properties in the whole membrane separation performance was evidenced.

Additionally, the functionalization of MOFs can possibly improve the interaction of the MOF with the polyamide, which can further change the performance of membranes. However, as the water passes through the TFN membranes primarily in the channels of MIL-101(Cr), the selective nanochannels inside the MOF, which dominated the separation property of the whole composite membrane, are therefore primarily responsible for the high-performance of the ED-TFN membrane for efficiently rejecting charged solutes.

Rejection of Charged PhACs. Figure 5a presents the rejection of charged PhACs by NFcontrol and various MOF-TFN membranes. The incorporation of MIL-101(Cr), ED-MIL-101(Cr) and AMSA-MIL-101(Cr) all improved membrane rejection for $PhACs^+$ but by

different extents. The rejection rates against terbutaline, atenolol and fluoxitine by MIL-TFN membrane were 70.8%, 79.1% and 87.3%, respectively. These values were higher than those of NFcontrol (56.5%, 73.2% and 79.5%, respectively). The moderate improvement is ascribed to the positively charged nature of Cr CUSs, but the charge was apparently not strong enough to effectively reject $PhACs^+$. In comparison, the highest rejection was achieved by ED-TFN membrane, with rejection rates against terbutaline, atenolol and fluoxitine of 82.7%, 90.1% and 92.7%, respectively. The ED-TFN presented nearly 2 times larger water/$PhACs^+$ selectivity (*e.g.*, A/B_{atenolol}) compared to MIL-TFN membrane and 4 times compared to NFcontrol membrane (Figure 5b). These results demonstrate the effectiveness of dually charged nanochannels for enhancing the removal of charged PhACs. Compared with the typical zwitterionic membranes that also have the potential to increase the rejection of both $PhAC^+$ and $PhAC^-$ but may compromise water permeance[21], the ED-TFN membrane can simultaneously obtain high rejection rate and significantly increased water permeability, which suggests the great potential of ED-TFN membrane for efficient removal of PhACs with relatively low energy consumption in wastewater reclamation.

The rejections of $PhACs^+$ by AMSA-TFN membrane were higher than those of NFcontrol but lower than MIL-TFN, further indicating the important role of grafted functional group. For $PhACs^-$, the rejection rate by MOF-TFN membranes was maintained at high level of ~90%, indicative of the electrostatic repulsion between deprotonated carboxyl groups outside MOFs and $PhACs^-$.

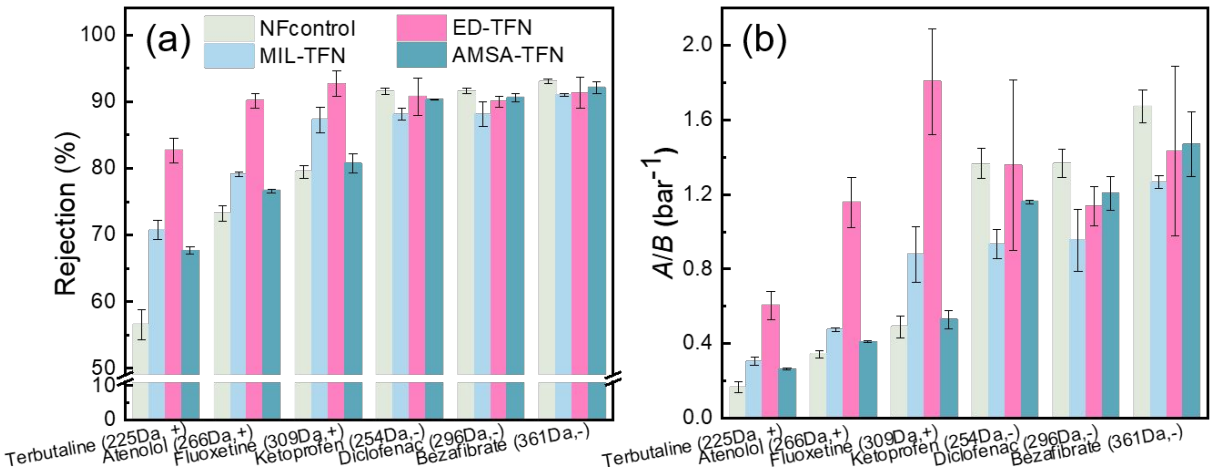

Figure 5. (a) Rejection and (b) selectivity (*A/B*) of charged PhACs (200 μg/L) of NFcontrol and TFN membrane loaded with different MOFs.

Interaction between PhACs and MOFs. We tried to further reveal the mechanisms of improved rejection of charged PhACs by nanochannels of ED-MIL-101(Cr), via probing interaction between PhACs and MOFs by a typical sorption test (Section S10)**.** The ED-MIL-101(Cr) showed more sorption for $PhAC^-$ than those of MIL-101(Cr) and ASMA-MIL-101(Cr). This tendency corresponds well to the literature[47], where ED grafted MIL-101(Cr) showed more sorption of naproxen and clofibric acid over those of MIL-101(Cr) and ASMA-MIL-101(Cr). In contrast, the ED-MIL-101(Cr) showed less sorption for $PhAC^+$ than those of MIL-101(Cr) and ASMA-MIL-101(Cr), indicative of an increased electrostatic repulsion between $PhAC^+$ and ED-MIL-101(Cr). The change of sorption behavior after grafting is consistent with the data of zeta potential (Figure S8). This suggests that the sorption behavior can somewhat reflect the bulk charge of MOFs but the dually charge nature (for filtration) of MOFs (especially for ED-MIL-101(Cr)) cannot be thoroughly revealed by sole sorption experiment.

Therefore, to further illustrate the mechanisms of rejection of charged PhACs by ED-TFN

membrane, we conducted DFT based molecular simulations with solvent model to quantify the interaction between ED-MIL-101(Cr), *i.e.*, the primary nanochannel of ED-TFN membrane, and charged PhACs including ketoprofen (-) and atenolol (+) at neutral pH. The solvent in the DFT calculation was set as water. The possible bonding sites, interatomic distance between PhACs and functional groups, and the repulsion energy were calculated, with the results shown in Figures 6a, b. The carboxyl groups outside the MOF shows higher repulsion energy to ketoprofen (-) than the amine group inside the pores (Figure 6a), and the primary contributor to the repulsion energy to atenolol (+) is the amine group (Figure 6b). Furthermore, the molecular migration energy barriers of the two PhACs across the ED-MIL-101(Cr) were calculated (Figure 6c) also with background solvent set as water. In the migration energy calculation, the possible contribution of electrostatic interaction, π-π interaction, hydrogen bonding, and direct coordination were all considered. The highest value of the migration energy barriers of positively and negatively charged PhACs both reached nearly 2~3 eV (Figure 6d), which represented a high energy barrier of the structure of ED-MIL-101(Cr) for the two PhACs to pass through.[48,49] The migration energy barrier of atenolol (+) through ED-MIL-101(Cr) is higher than that of pristine MIL-101(Cr) (Figure S12), indicating the necessity of grafting ED for effective removal of both positively and negatively charged PhACs.

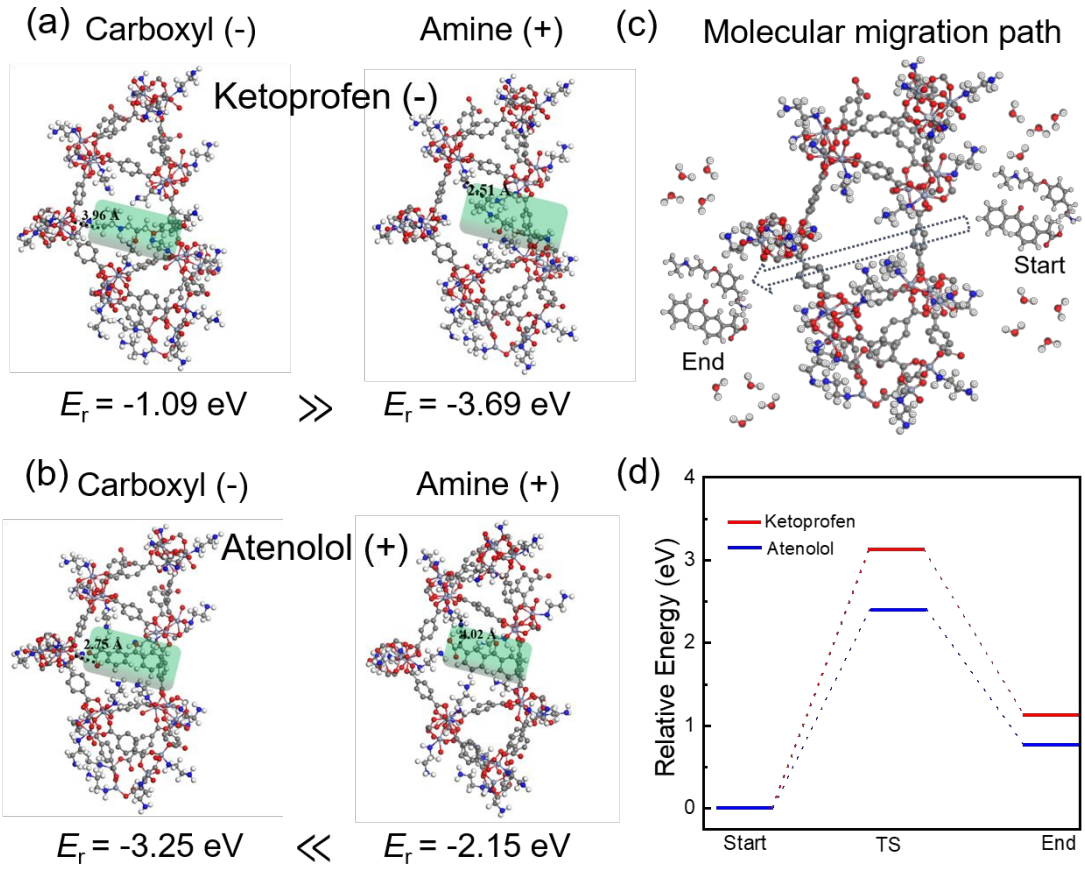

Figure 6. Interactions between ED-MIL-101(Cr) and charged PhACs by density functional theory calculation: (a, b) Repulsion energy; (c, d) Migration energy barrier of charged PhACs across the ED-MIL-101(Cr).

Implications for Wastewater Reclamation. Traditional polyamide-based TFC membranes often have insufficient rejection of some positively charged or hydrophobic organic micropollutants[18,50,51]. In this study, the dually charged ED-MIL-101(Cr) incorporated TFN membrane showed significantly higher rejection of $PhACs^+$ without losing the rejection of $PhACs^-$ and water permeability. Moreover, introducing ED-MIL-101(Cr) can also form hydrophilic nanochannels in the MOF-TFN membrane (Figure S13), which can improve the rejection rate against hydrophobic organic micropollutants according to our previous study[24]

397 thanks to the hydrophilic selective nanochannels. Therefore, the ED-TFN membrane has a great
398 potential for effective removal of a wider spectrum of organic micropollutants, providing a
399 promising way for highly selective and efficient wastewater reclamation.

400 The fouling propensity is also a primary concern for membrane-based wastewater
401 reclamation[52,53]. Tuning the charge of the bulk membrane surface from negative to positive not
402 only potentially loses the rejection rate of PhACs$^-$, but also increases the fouling tendency as
403 most of the foulants are negatively charged and easily deposited on the bulk positive surface
404 via electrostatic attraction[54]. Our dually charged MOF-TFN membrane based on the
405 manipulation of primary nanochannels, *i.e.*, the pores of ED-MIL-101(Cr), can enable the
406 rejection of both positively and negatively charged PhACs without changing the net negatively
407 charged surface. The negatively charged and more hydrophilic surface enables low fouling
408 propensity than the bulk positively charged surface, highlighting superior performance for
409 wastewater reclamation by the MOF-TFN membrane.

410

411 ## ASSOCIATED CONTENT

412 **Supporting information**

413 The Supporting Information is available free of charge on the ACS Publications website at DOI:
414 S1, Profile of MOFs used; S2, Physicochemical properties and analytical method of selected
415 charged PhACs; S3, Chemical structures constructed in DFT calculation; S4, BET
416 characterizations of pristine and grafted MIL-101(Cr); S5, XPS characterization of various
417 membranes; S6, Transport properties of membranes; S7, Charge properties of surface of
418 membranes; S8, Dextrose (180 Da) rejections by membranes; S9, Gold nanoparticle filtration

tests of MIL-TFN and AMSA-TFN; S10, Sorption of PhACs by pristine and grafted MIL-101(Cr); S11, Migration energy barrier of charged PhACs across MIL-101(Cr); S12, Water contact angle characterizations of various membranes.

AUTHOR INFORMATION

Corresponding Author

*Tel.: +86-21-65975669, Fax: +86-21-65980400, E-mail address: zwwang@tongji.edu.cn

Notes

The authors declare no completing financial interest.

ACKNOWLEDGEMENT

We thank the National Natural Science Foundation of China (grants 51838009 & 51925806), and the Peak Discipline Construction Program in Environment and Ecology of Shanghai for the financial support of the work.

REFERENCES

(1) Shannon, M. A.; Bohn, P. W.; Elimelech, M.; Georgiadis, J. G.; Mariñas, B. J.; Mayes, A. M. Science and Technology for Water Purification in the Coming Decades. *Nature* **2008**, *452* (7185), 301–310. https://doi.org/10.1038/nature06599.

(2) Hering, J. G.; Ingold, K. M. Water Resources Management: What Should Be Integrated? *Science* **2012**, *336* (6086), 1234–1235. https://doi.org/10.1126/science.1218230.

(3) Cheng, H.; Hu, Y.; Zhao, J. Meeting China's Water Shortage Crisis: Current Practices and Challenges. *Environmental Science & Technology* **2009**, *43* (2), 240–244. https://doi.org/10.1021/es801934a.

(4) Yangali-Quintanilla, V.; Maeng, S. K.; Fujioka, T.; Kennedy, M.; Amy, G. Proposing Nanofiltration as Acceptable Barrier for Organic Contaminants in Water Reuse. *Journal of Membrane Science* **2010**, *362* (1–2), 334–345. https://doi.org/10.1016/j.memsci.2010.06.058.

(5) Tang, C. Y.; Yang, Z.; Guo, H.; Wen, J. J.; Nghiem, L. D.; Cornelissen, E. Potable Water Reuse through Advanced Membrane Technology. *Environmental Science & Technology* **2018**, *52* (18),

10215–10223. https://doi.org/10.1021/acs.est.8b00562.

(6) Schwarzenbach, R. P.; Escher, B. I.; Fenner, K.; Hofstetter, T. B.; Johnson, C. A.; Gunten, U. von; Wehrli, B. The Challenge of Micropollutants in Aquatic Systems. *Science* **2006**, *313* (5790), 1072–1077. https://doi.org/10.1126/science.1127291.

(7) Zhang, R.; Meng, T.; Huang, C.-H.; Ben, W.; Yao, H.; Liu, R.; Sun, P. PPCP Degradation by Chlorine–UV Processes in Ammoniacal Water: New Reaction Insights, Kinetic Modeling, and DBP Formation. *Environmental Science & Technology* **2018**, *52* (14), 7833–7841. https://doi.org/10.1021/acs.est.8b00094.

(8) Kosma, C. I.; Lambropoulou, D. A.; Albanis, T. A. Investigation of PPCPs in Wastewater Treatment Plants in Greece: Occurrence, Removal and Environmental Risk Assessment. *Science of The Total Environment* **2014**, *466–467*, 421–438. https://doi.org/10.1016/j.scitotenv.2013.07.044.

(9) Dai, G.; Huang, J.; Chen, W.; Wang, B.; Yu, G.; Deng, S. Major Pharmaceuticals and Personal Care Products (PPCPs) in Wastewater Treatment Plant and Receiving Water in Beijing, China, and Associated Ecological Risks. *Bulletin Environmental Contamination and Toxicology* **2014**, *92* (6), 655–661. https://doi.org/10.1007/s00128-014-1247-0.

(10) Pomati, F.; Castiglioni, S.; Zuccato, E.; Fanelli, R.; Vigetti, D.; Rossetti, C.; Calamari, D. Effects of a Complex Mixture of Therapeutic Drugs at Environmental Levels on Human Embryonic Cells. *Environmental Science & Technology* **2006**, *40* (7), 2442–2447. https://doi.org/10.1021/es051715a.

(11) Mohammad, A. W.; Teow, Y. H.; Ang, W. L.; Chung, Y. T.; Oatley-Radcliffe, D. L.; Hilal, N. Nanofiltration Membranes Review: Recent Advances and Future Prospects. *Desalination* **2015**, *356*, 226–254. https://doi.org/10.1016/j.desal.2014.10.043.

(12) Boo, C.; Wang, Y.; Zucker, I.; Choo, Y.; Osuji, C. O.; Elimelech, M. High Performance Nanofiltration Membrane for Effective Removal of Perfluoroalkyl Substances at High Water Recovery. *Environmental Science & Technology* **2018**, *52* (13), 7279–7288. https://doi.org/10.1021/acs.est.8b01040.

(13) Garcia-Ivars, J.; Martella, L.; Massella, M.; Carbonell-Alcaina, C.; Alcaina-Miranda, M.-I.; Iborra-Clar, M.-I. Nanofiltration as Tertiary Treatment Method for Removing Trace Pharmaceutically Active Compounds in Wastewater from Wastewater Treatment Plants. *Water Research* **2017**, *125*, 360–373. https://doi.org/10.1016/j.watres.2017.08.070.

(14) Fathizadeh, M.; Ngoc Tien, H.; Khivantsev, K.; Chen, J.-T.; Yu, M. Printing Ultrathin Graphene Oxide Nanofiltration Membranes for Water Purification. *Journal of Materials Chemistry A* **2017**, *5* (39), 20860–20866. https://doi.org/10.1039/C7TA06307E.

(15) Khanzada, N. K.; Farid, M. U.; Kharraz, J. A.; Choi, J.; Tang, C. Y.; Nghiem, L. D.; Jang, A.; An, A. K. Removal of Organic Micropollutants Using Advanced Membrane-Based Water and Wastewater Treatment: A Review. *Journal of Membrane Science* **2019**, 298: 117672. https://doi.org/10.1016/j.memsci.2019.117672.

(16) Nghiem, L. D.; Schäfer, A. I.; Elimelech, M. Pharmaceutical Retention Mechanisms by Nanofiltration Membranes. *Environmental Science & Technology* **2005**, *39* (19), 7698–7705. https://doi.org/10.1021/es0507665.

(17) Nghiem, L. D.; Schäfer, A. I.; Elimelech, M. Role of Electrostatic Interactions in the Retention of Pharmaceutically Active Contaminants by a Loose Nanofiltration Membrane. *Journal of Membrane Science* **2006**, *286* (1–2), 52–59. https://doi.org/10.1016/j.memsci.2006.09.011.

(18) Verliefde, A. R. D.; Cornelissen, E. R.; Heijman, S. G. J.; Verberk, J. Q. J. C.; Amy, G. L.; Van der Bruggen, B.; van Dijk, J. C. The Role of Electrostatic Interactions on the Rejection of Organic Solutes

in Aqueous Solutions with Nanofiltration. *Journal of Membrane Science* **2008**, *322* (1), 52–66. https://doi.org/10.1016/j.memsci.2008.05.022.

(19) Lin, Y.-L.; Chiou, J.-H.; Lee, C.-H. Effect of Silica Fouling on the Removal of Pharmaceuticals and Personal Care Products by Nanofiltration and Reverse Osmosis Membranes. *Journal of Hazardous Materials* **2014**, *277*, 102–109. https://doi.org/10.1016/j.jhazmat.2014.01.023.

(20) Ouyang, Z.; Huang, Z.; Tang, X.; Xiong, C.; Tang, M.; Lu, Y. A Dually Charged Nanofiltration Membrane by PH-Responsive Polydopamine for Pharmaceuticals and Personal Care Products Removal. *Separation and Purification Technology* **2019**, *211*, 90–97. https://doi.org/10.1016/j.seppur.2018.09.059.

(21) de Grooth, J.; Reurink, D. M.; Ploegmakers, J.; de Vos, W. M.; Nijmeijer, K. Charged Micropollutant Removal With Hollow Fiber Nanofiltration Membranes Based On Polycation/Polyzwitterion/Polyanion Multilayers. *ACS Appl. Mater. Interfaces* **2014**, *6* (19), 17009–17017. https://doi.org/10.1021/am504630a.

(22) Darling, S. B. Perspective: Interfacial Materials at the Interface of Energy and Water. *Journal of Applied Physics* **2018**, *124* (3), 030901. https://doi.org/10.1063/1.5040110.

(23) Jeong, B.-H.; Hoek, E. M. V.; Yan, Y.; Subramani, A.; Huang, X.; Hurwitz, G.; Ghosh, A. K.; Jawor, A. Interfacial Polymerization of Thin Film Nanocomposites: A New Concept for Reverse Osmosis Membranes. *Journal of Membrane Science* **2007**, *294* (1–2), 1–7. https://doi.org/10.1016/j.memsci.2007.02.025.

(24) Dai, R.; Guo, H.; Tang, C. Y.; Chen, M.; Li, J.; Wang, Z. Hydrophilic Selective Nanochannels Created by Metal Organic Frameworks in Nanofiltration Membranes Enhance Rejection of Hydrophobic Endocrine-Disrupting Compounds. *Environmental Science & Technology* **2019**, *53* (23), 13776–13783. https://doi.org/10.1021/acs.est.9b05343.

(25) Yang, Z.; Guo, H.; Yao, Z.; Mei, Y.; Tang, C. Y. Hydrophilic Silver Nanoparticles Induce Selective Nanochannels in Thin Film Nanocomposite Polyamide Membranes. *Environmental Science & Technology* **2019**, acs.est.9b00473. https://doi.org/10.1021/acs.est.9b00473.

(26) Ferey, G. A Chromium Terephthalate-Based Solid with Unusually Large Pore Volumes and Surface Area. *Science* **2005**, *309* (5743), 2040–2042. https://doi.org/10.1126/science.1116275.

(27) Yang, H.-C.; Hou, J.; Chen, V.; Xu, Z.-K. Janus Membranes: Exploring Duality for Advanced Separation. *Angewandte Chemie International Edition* **2016**, *55* (43), 13398–13407. https://doi.org/10.1002/anie.201601589.

(28) Yang, H.-C.; Xie, Y.; Hou, J.; Cheetham, A. K.; Chen, V.; Darling, S. B. Janus Membranes: Creating Asymmetry for Energy Efficiency. *Advanced Materials* **2018**, *30* (43), 1801495. https://doi.org/10.1002/adma.201801495.

(29) Wang, S.; Bromberg, L.; Schreuder-Gibson, H.; Hatton, T. A. Organophophorous Ester Degradation by Chromium(III) Terephthalate Metal–Organic Framework (MIL-101) Chelated to N,N-Dimethylaminopyridine and Related Aminopyridines. *ACS Applied Materials & Interfaces* **2013**, *5* (4), 1269–1278. https://doi.org/10.1021/am302359b.

(30) Hwang, Y. K.; Hong, D.-Y.; Chang, J.-S.; Jhung, S. H.; Seo, Y.-K.; Kim, J.; Vimont, A.; Daturi, M.; Serre, C.; Férey, G. Amine Grafting on Coordinatively Unsaturated Metal Centers of MOFs: Consequences for Catalysis and Metal Encapsulation. *Angewandte Chemie International Edition* **2008**, *47* (22), 4144–4148. https://doi.org/10.1002/anie.200705998.

(31) Hong, D.-Y.; Hwang, Y. K.; Serre, C.; Férey, G.; Chang, J.-S. Porous Chromium Terephthalate MIL-101 with Coordinatively Unsaturated Sites: Surface Functionalization, Encapsulation, Sorption and

Catalysis. *Advanced Functional Materials* **2009**, *19* (10), 1537–1552. https://doi.org/10.1002/adfm.200801130.

(32) Ahmed, I.; Hasan, Z.; Khan, N. A.; Jhung, S. H. Adsorptive Denitrogenation of Model Fuels with Porous Metal-Organic Frameworks (MOFs): Effect of Acidity and Basicity of MOFs. *Applied Catalysis B: Environmental* **2013**, *129*, 123–129. https://doi.org/10.1016/j.apcatb.2012.09.020.

(33) Dai, R.; Zhang, X.; Liu, M.; Wu, Z.; Wang, Z. Porous Metal Organic Framework CuBDC Nanosheet Incorporated Thin-Film Nanocomposite Membrane for High-Performance Forward Osmosis. *Journal of Membrane Science* **2019**, *573*, 46–54. https://doi.org/10.1016/j.memsci.2018.11.075.

(34) Guo, H.; Yao, Z.; Yang, Z.; Ma, X.; Wang, J.; Tang, C. Y. A One-Step Rapid Assembly of Thin Film Coating Using Green Coordination Complexes for Enhanced Removal of Trace Organic Contaminants by Membranes. *Environmental Science & Technology* **2017**, *51* (21), 12638–12643. https://doi.org/10.1021/acs.est.7b03478.

(35) Zhao, S.; Yao, Y.; Ba, C.; Zheng, W.; Economy, J.; Wang, P. Enhancing the Performance of Polyethylenimine Modified Nanofiltration Membrane by Coating a Layer of Sulfonated Poly(Ether Ether Ketone) for Removing Sulfamerazine. *Journal of Membrane Science* **2015**, *492*, 620–629. https://doi.org/10.1016/j.memsci.2015.03.017.

(36) Ben, W.; Zhu, B.; Yuan, X.; Zhang, Y.; Yang, M.; Qiang, Z. Occurrence, Removal and Risk of Organic Micropollutants in Wastewater Treatment Plants across China: Comparison of Wastewater Treatment Processes. *Water Research* **2018**, *130*, 38–46. https://doi.org/10.1016/j.watres.2017.11.057.

(37) Zhang, Q.-Q.; Ying, G.-G.; Pan, C.-G.; Liu, Y.-S.; Zhao, J.-L. Comprehensive Evaluation of Antibiotics Emission and Fate in the River Basins of China: Source Analysis, Multimedia Modeling, and Linkage to Bacterial Resistance. *Environmental Science & Technology* **2015**, *49* (11), 6772–6782. https://doi.org/10.1021/acs.est.5b00729.

(38) Guo, H.; Deng, Y.; Tao, Z.; Yao, Z.; Wang, J.; Lin, C.; Zhang, T.; Zhu, B.; Tang, C. Y. Does Hydrophilic Polydopamine Coating Enhance Membrane Rejection of Hydrophobic Endocrine-Disrupting Compounds? *Environmental Science & Technology Letters* **2016**, *3* (9), 332–338. https://doi.org/10.1021/acs.estlett.6b00263.

(39) Krishnan, K.; Plane, R. A. Raman and Infrared Spectra of Complexes of Ethylenediamine with Zinc(II), Cadmium(II), and Mercury(II). *Inorganic Chemistry* **1966**, *5* (5), 852–857. https://doi.org/10.1021/ic50039a031.

(40) Young, D. A.; Freedman, T. B.; Lipp, E. D.; Nafie, L. A. Vibrational Circular Dichroism in Transition-Metal Complexes. 2. Ion Association, Ring Conformation, and Ring Currents of Ethylenediamine Ligands. *Journal of the American Chemical Society* **1986**, *108* (23), 7255–7263. https://doi.org/10.1021/ja00283a021.

(41) Chen, C.; Zhang, M.; Guan, Q.; Li, W. Kinetic and Thermodynamic Studies on the Adsorption of Xylenol Orange onto MIL-101(Cr). *Chemical Engineering Journal* **2012**, *183*, 60–67. https://doi.org/10.1016/j.cej.2011.12.021.

(42) Ramon, G. Z.; Hoek, E. M. V. Transport through Composite Membranes, Part 2: Impacts of Roughness on Permeability and Fouling. *Journal of Membrane Science* **2013**, *425–426*, 141–148. https://doi.org/10.1016/j.memsci.2012.08.004.

(43) Song, X.; Gan, B.; Qi, S.; Guo, H.; Tang, C. Y.; Zhou, Y.; Gao, C. Intrinsic Nanoscale Structure of Thin Film Composite Polyamide Membranes: Connectivity, Defects, and Structure–Property Correlation. *Environmental Science & Technology* **2020**, *54* (6), 3559–3569.

https://doi.org/10.1021/acs.est.9b05892.

(44) Yang, Z.; Guo, H.; Tang, C. Y. The Upper Bound of Thin-Film Composite (TFC) Polyamide Membranes for Desalination. *Journal of Membrane Science* **2019**, *590*, 117297. https://doi.org/10.1016/j.memsci.2019.117297.

(45) Luo, J.; Wan, Y. Effects of PH and Salt on Nanofiltration—a Critical Review. *Journal of Membrane Science* **2013**, *438*, 18–28. https://doi.org/10.1016/j.memsci.2013.03.029.

(46) Szoke, S.; Patzay, G.; Weiser, L. Characteristics of Thin-Film Nanofiltration Membranes at Various PH-Values. *Desalination* **2003**, *151* (2), 123–129. https://doi.org/10.1016/S0011-9164(02)00990-6.

(47) Hasan, Z.; Choi, E.-J.; Jhung, S. H. Adsorption of Naproxen and Clofibric Acid over a Metal–Organic Framework MIL-101 Functionalized with Acidic and Basic Groups. *Chemical Engineering Journal* **2013**, *219*, 537–544. https://doi.org/10.1016/j.cej.2013.01.002.

(48) Ehemann, R. C.; Krstić, P. S.; Dadras, J.; Kent, P. R.; Jakowski, J. Detection of Hydrogen Using Graphene. *Nanoscale Research Letters* **2012**, *7* (1), 198. https://doi.org/10.1186/1556-276X-7-198.

(49) Tsetseris, L.; Pantelides, S. T. Graphene: An Impermeable or Selectively Permeable Membrane for Atomic Species? *Carbon* **2014**, *67*, 58–63. https://doi.org/10.1016/j.carbon.2013.09.055.

(50) Verliefde, A. R. D.; Cornelissen, E. R.; Heijman, S. G. J.; Hoek, E. M. V.; Amy, G. L.; Bruggen, B. V. der; van Dijk, J. C. Influence of Solute−Membrane Affinity on Rejection of Uncharged Organic Solutes by Nanofiltration Membranes. *Environmental Science & Technology* **2009**, *43* (7), 2400–2406. https://doi.org/10.1021/es803146r.

(51) Bendavid, A.; Bason, S.; Jopp, J.; Oren, Y.; Freger, V. Partitioning of Organic Solutes between Water and Polyamide Layer of RO and NF Membranes: Correlation to Rejection. *Journal of Membrane Science* **2006**, *281* (1–2), 480–490. https://doi.org/10.1016/j.memsci.2006.04.017.

(52) Tin, M. M. M.; Anioke, G.; Nakagoe, O.; Tanabe, S.; Kodamatani, H.; Nghiem, L. D.; Fujioka, T. Membrane Fouling, Chemical Cleaning and Separation Performance Assessment of a Chlorine-Resistant Nanofiltration Membrane for Water Recycling Applications. *Separation and Purification Technology* **2017**, *189*, 170–175. https://doi.org/10.1016/j.seppur.2017.07.080.

(53) Lee, S.; Ang, W. S.; Elimelech, M. Fouling of Reverse Osmosis Membranes by Hydrophilic Organic Matter: Implications for Water Reuse. *Desalination* **2006**, *187* (1), 313–321. https://doi.org/10.1016/j.desal.2005.04.090.

(54) Wang, Z.; Ma, J.; Tang, C. Y.; Kimura, K.; Wang, Q.; Han, X. Membrane Cleaning in Membrane Bioreactors: A Review. *Journal of Membrane Science* **2014**, *468*, 276–307. https://doi.org/10.1016/j.memsci.2014.05.060.